Seismic Anisotropy of Silica Nanostructure Polymorph under High-Pressure of the Earth's Mantle Condition

Saliha Belabas [1], Khalissa Layadi[2], Zohir Radi*[2], Mahmoud Hamlaoui[3], Amar Mosbah[1]

[1]Physics Department, Faculty of Sciences, Ferhat Abbas University, Sétif, Algeria

[2]Center for Research in Astronomy, Astrophysics and Geophysics, Algeria

[3]Institute of Architecture and Earth Science, Ferhat Abbas University, Sétif, Algeria

Author Correspondenceemail: z.radi@craag.dz

Received: 05/ 2023; Accepted: 07/2023; Published: 08/ 2023

Abstract

In this study, the elastic P-wave and S-wave, velocities, V_P and Vs, and seismic anisotropies of two high-pressure polymorphs of silica, stishovite and $CaCl_2$-type, were estimated in the 0-80 GPa high-pressure domain of the earth's mantle at zero temperature from their elastic constants computed from density functional theory. Our obtained results showed that Vs varies very little with pressure, from 7.1 (at 10 GPa) to 7.9 (at 80 GPa) km/s, whereas the variation of V_P is significant, ranges from 11.5 to 13.5 km/s. The azimuthal anisotropy variation showed that the S-wave is more strongly anisotropic than the P-wave, with a decrease of 60 and 10% at 40 GPa phase transition pressure, respectively. The obtained results may be relevant in understanding the deep Earth structure from the geophysical implications of the stishovite and $CaCl_2$-type transformations.

Keywords: high-pressure; elastic body wave; azimuthal anisotropy; stishovite; CaCl2-type; SiO2.

Tob Regul Sci.™ 2023;9(1): 4141-4153
DOI: doi.org/10.18001/TRS.9.290

I.Introduction

Studying Earth's minerals with theoretical and experimental approaches plays a very important role in understanding the deep Earth structure, including chemical composition, discontinuities, seismic wave propagation, density, and plate tectonic motions (subduction, mid-oceanic divergence, etc.). The combination of mineral studies and seismological observations can provide more precision. One of the most chemical elements in the primitive mantle is silica, SiO_2, with a composition of 46 wt%; ([1]). It may exist in ocean lithospheric slabs as a result of mid-oceanic ridge basalt (MORB), which forms at divergent plate boundaries and distorts the pressure and temperature conditions of the lower mantle. In the present study, we focus on stishovite and

$CaCl_2$-type phases (from 0 to 300 GPa, six high-pressure transformations of SiO_2 are quartz, coesite, stishovite, $CaCl_2$-type, seifertite (α-PbO_2-type), and pyrite; [2]). The MORB geochemical composition contains 15–19 wt% of stishovite at 40–60 GPa and 2100 K, and the crust lithospheric slab contains a higher proportion of it ([3]). The phase transition pressure of the stishovite to the orthorhombic $CaCl_2$-type phase can be a useful parameter to determine the slab discontinuity. The corresponding phase transition pressure (and/or P-t diagram) is converted to the earth's mantle depth and then attributed to this discontinuity, which cannot be detected using seismological observation ([3], [4]).

From the geophysical implication proposed by [5], the stishovite- $CaCl_2$ phase transition occurs at 1180 km depth (equivalent to 47 GPa) in the lower mantle, where compressional, P, and shear, S, wave velocities V_P and Vs increase by 20 (13 km/s) and 60% (7 km/s) respectively, compared to 1-2% only changes associated with the $CaCl_2$-seifertite phase transition. According to the same authors, this is due to large changes in elastic properties. From the phase diagram of [6], the $CaCl_2$-type phase is stable in the P-t field between the stishovite-$CaCl_2$-type and $CaCl_2$-seifertite boundaries, defined P=56.1 +0.00585*T (K) and P=106.3 +0.00579*T (K) GPa, respectively, where the pressure varies very little compared to the temperature. Also, it means that $CaCl_2$-type is abundant just before the core-mantle boundary, which corresponds to 2891 km based on the depth-pressure of the Earth's structure reported by [7]. From the review of [3], the phase transition pressure of the stishovite-$CaCl_2$-type varies between 50 and 80 GPa, but the boundary in the P-t diagram is unresolved. The phase transition from the $CaCl_2$-type to seifertite is strongly dependent on the starting material observed by [4] from their experimental investigation based on X-ray diffraction in laser-heated diamond anvil cells.

The importance of elastic properties in the study of mantle materials plays a great role in geophysics. It appears in the seismological parameters (V_P, Vs, density, etc.) of the earth's interior determination with the different main discontinuities between its regions (e.g., [8], [9], [10]). According to [11], the lower mantle makes up 55% of the earth's volume. Therefore, it dominates energy transport in the deep interior and may have an influence on the planet's thermal and chemical evolution. It is topped by the upper mantle, which is composed of two main layers: one rigid and one plastic. Seismic anisotropy analysis showed that the lithosphere is anisotropic, whereas the asthenosphere is isotropic. The explanation of anisotropy's origin is different from the lithosphere's origin itself, which is oceanic and continental. In the oceanic lithosphere, it develops in response to the alignment of olivine and pyroxene, and in the continental lithosphere, it appears to be caused by a strain-induced preferred orientation of anisotropic crystals such as olivine ([1]). For examples of seismic anisotropy, [8] used the S-wave splitting technique to define the azimuth of the fast S-wave and relate it to the direction of African plate motion.

The presence of stishovite can be an indicator of the presence of subducted oceanic crust in the lower mantle by distorting to adapt to higher pressures and becoming elastically softer. At this depth or pressure of distortion, the shear wave velocities may be slowed down when they travel through this elastically soft and compressible area [12]. Large and precise knowledge of the structure of the earth's interior from physical property determination combined with geophysical observations can explain the origins of seismic anisotropy, thermal and velocity anomalies, and convection in the upper mantle and the relationship with the lower mantle at the 660 km discontinuity.

The current work is a continuation of the investigation of [13], which focused on the phase transition definition and elastic properties computation of the stishovite and $CaCl_2$-type polymorphs in 0-80 GPa using Density Functional Theory (DFT; [14]). In this one, a theoretical estimation of the high-pressure dependency of V_P, Vs of the two indicated phases from 0-80 GPa is done using the Christoffel tensor equation. The azimuthal anisotropy of body wave velocities is caused by their dependence on propagation direction. As a result, we examined the azimuthal anisotropies of P and S wave variation in the same pressure domain in order to quantify the propagation direction with pressure dependence in percentage terms.

II.Computation Details

In order to estimate the theoretical V_P and Vs in 0-80 GPa high pressure of the stishovite and $CaCl_2$-type phases of SiO_2, we considered the following formulas based on the pressure dependence of bulk modulus, B, shear modulus, G, and density, ρ, from [13]. We review the key components approach and results of [13] before delving into the computation of V_P and Vs, as well as the associated anisotropies and pressure dependency of the current work.

$$V_P = \sqrt{(B + \frac{4}{3}G)/\rho} \quad (1)$$

$$V_s = \sqrt{G/\rho} \quad (2)$$

II.1. Phase Transition Boundary and Elastic properties

To understand the seismic properties of silica, the elastic properties of silica under high pressure that correlate to the mantle depth condition are required. Reference [13] used DFT from the generalized gradient approach of first-principles techniques proposed by [12] in the Cambridge Serial Total Energy Package code (CASTEP; [14, 15]) to analyze the elastic characteristics of stishovite and $CaCl_2$-type phases. The DFT calculates total energy and forces and insists on finding the best geometries for atomic systems. Reference [13] employed the enthalpy difference technique from Gibbs free energy (e.g., [3]) to calculate the phase transition limit from stishovite

to $CaCl_2$-type phase, which was determined to be at 40 GPa. The enthalpy of stishovite and $CaCl_2$-type phases is plotted with pressure domain values in Fig. 1.

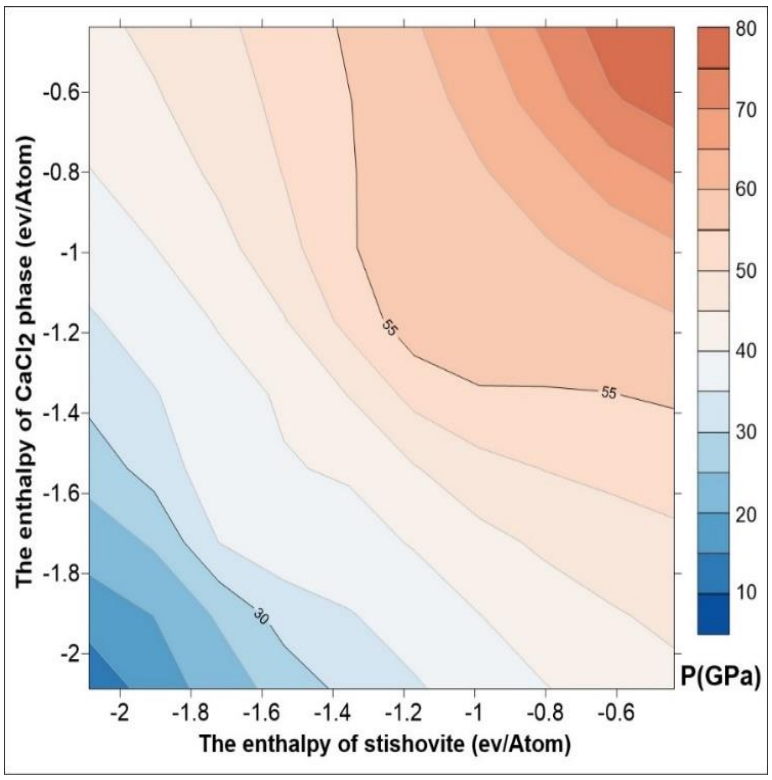

Fig. 1: The enthalpy of $CaCl_2$-type phase variation with thus of stishovite and pressure (color palette), showing a kind of linear relation between then in 40-45 GPa defined as phase transition limit inspired from [13].

It is shown that the variation between both polymorphs is more inclined for high-pressure values (greater than 45 GPa), then the behavior becomes quasi-linear in 40-45 GPa, and that the dependence returns to an inclined state below this pressure domain. This number is consistent with findings by [19] and [5]. According to [3], the phase transition from stishovite to $CaCl_2$-type phase occurs between 50 to 80 GPa, and the location and slope of the phase border are unresolved for pressure-temperature estimation.

The density-pressure dependency is represented in Fig. 2 by the elementary molecular volume, V, over the equilibrium volume, V_0, ratio, which shows that increasing density for high-pressure values induces a large reduction in V/V_0 with a positive slope of approximately. The fluctuation of V/V_0 at low pressures is produced by a slight variation in density separated by 40-45 GPa from the initial behavior (Fig. 2). This directly affects V_P and Vs from formulas (1) and (2).

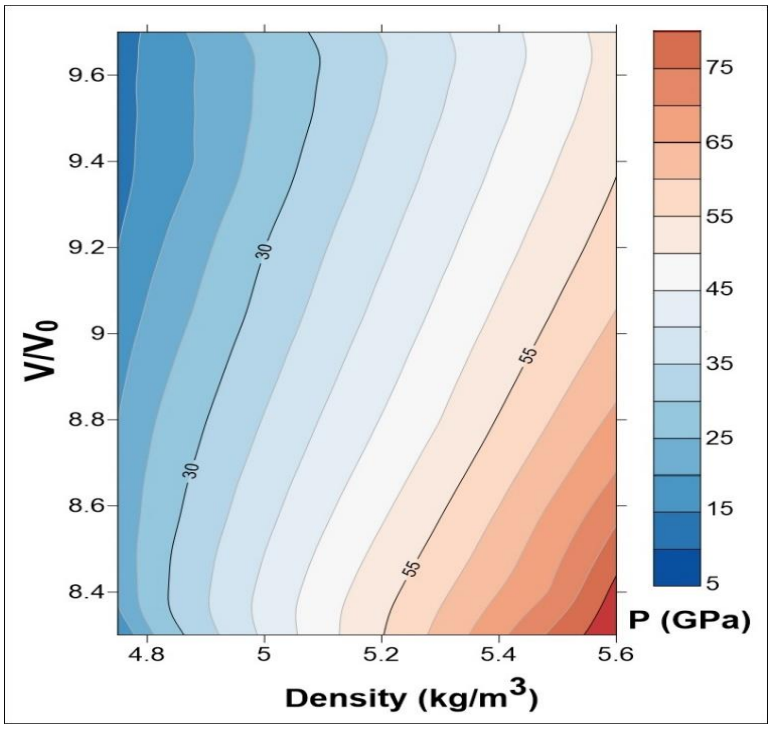

Fig. 2: Density and the elementary molecular volume, V, over the equilibrium volume, V_0, ratio dependence with pressure variation inspired from [13].

The final figure inspired from [13], is the bulk, B, and shear, G, modulus pressure dependency, as well as the earth's interior depth, displayed in Fig. 3, which is required for our V_P and Vs computation in this study. The change of B with pressure and depth is faster than that of G, but G modulus exhibits a form of stability in 45-80 GPa, which corresponds to 1000-1800 GPa. This behavior influences Vs more than V_P in formulas (1) and (2) since the change of density in this pressure interval is weak, ranging from 5.1 to 5.6 kg/m^3 as illustrated in Fig. 2.

II.2. Body Wave Velocities and Azimuthal Anisotropy Computation Theory

As stated in the preceding section, the isotropic body wave velocity, V_P, and Vs variation, were estimated from the high-pressure dependence of B, G, and, as shown in Fig. 3. The V_P and Vs are the velocities averaged over all propagation directions as determined by formulas with elastic constants, Cjikl, as shown in Table 1.

The stishovite structure is tetragonal with six nonzero elastic constants, Cjikl, whereas the $CaCl_2$-type structure is orthorhombic with nine nonzero constants. The velocities are estimated along the directions L and T using the Christoffel tensor formula, Γil, demonstrating that they depend on the direction of propagation. The Christoffel tensor can be calculated using the following formula:

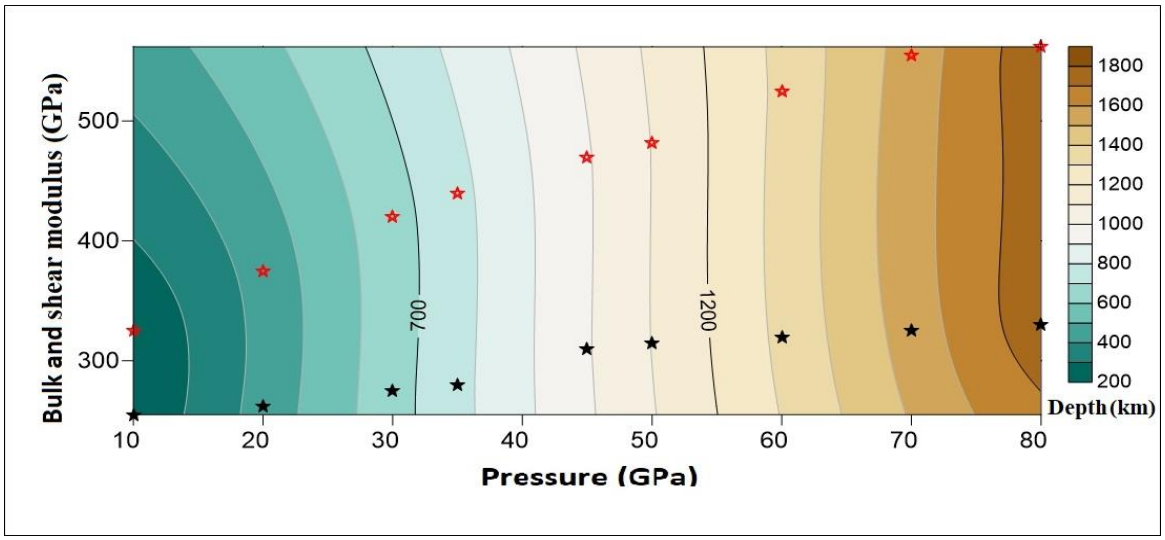

Fig. 3: Bulk (red stars) and shear (black stars) modulus variations in 0-80 GPa pressure and earth's interior depth from the model of [20] inspired from [13] computation.

$$\Gamma_{il} = C_{ijkl} * n_j * n_k \quad (3)$$

C_{ijkl} are elastic constants; n_j and n_k are unitary vectors with j and k directions.

Expanding the sum over the indices j and k, we found:

$$\Gamma_{il} = C_{i11l}n_1^2 + C_{i22l}n_2^2 + C_{i23l}n_3^2 + (C_{i12l} + C_{i21l})n_1n_2 + (C_{i13l} + C_{i31l})n_1n_3 + (C_{i23l} + C_{i32l})n_2n_3 \quad (4)$$

Hence the terms:

$$\Gamma_{11} = C_{11}n_1^2 + C_{66}n_2^2 + C_{55}n_3^2 + 2C_{16}n_1n_2 + 2C_{15}n_1n_3 + C_{56}n_2n_3 \quad (5)$$

$$\Gamma_{12} = C_{16}n_1^2 + C_{26}n_2^2 + C_{45}n_3^2 + (C_{12} + C_{66})n_1n_2 + (C_{14} + C_{56})n_1n_3 + (C_{46} + C_5)n_2n_3 \quad (6)$$

$$\Gamma_{13} = C_{15}n_1^2 + C_{46}n_2^2 + C_{35}n_3^2 + (C_{14} + C_{56})n_1n_2 + (C_{13} + C_{55})n_1n_3 + (C_{36} + C_{45})n_2n_3 \quad (7)$$

$$\Gamma_{22} = C_{66}n_1^2 + C_{22}n_2^2 + C_{44}n_3^2 + 2C_{26}n_1n_2 + 2C_{46}n_1n_3 + C_{24}n_2n_3 \quad (8)$$

$$\Gamma_{23} = C_{56}n_1^2 + C_{24}n_2^2 + C_{34}n_3^2 + (C_{46} + C_{25})n_1n_2 + (C_{36} + C_{45})n_1n_3 + (C_{23} + C_{44})n_2n_3 \quad (9)$$

$$\Gamma_{33} = C_{55}n_1^2 + C_{44}n_2^2 + C_{33}n_3^2 + 2C_{45}n_1n_2 + 2C_{35}n_1n_3 + C_{34}n_2n_3 \quad (10)$$

$$\Gamma_{21} = \Gamma_{12};\ \Gamma_{31} = \Gamma_{31};\ \Gamma_{32} = \Gamma_{23}$$

Given the tetragonal elastic constants, the elements of the Christoffel tensor are:

$$\Gamma_{11} = C_{11}n_1^2 + C_{66}n_2^2 + C_{55}n_3^2 \quad (11)$$

$$\Gamma_{12} = C_{16}(n_1^2 + n_2^2) + (C_{12} + C_{66})n_1n_2 \quad (12)$$

$$\Gamma_{13} = (C_{13} + C_{44})n_1n_3 \quad (13)$$

$$\Gamma_{22} = C_{66}n_1^2 + C_{11}n_2^2 + C_{44}n_3^2 \quad (14)$$

$$\Gamma_{23} = (C_{13} + C_{44})n_2n_3 \quad (15)$$

$$\Gamma_{33} = C_{44}(n_1^2 + n_2^2) + C_{33}n_3^2 \quad (16)$$

Table 1: Body wave velocities, V_P and V_S expressions depend on the longitudinal, L, and transversal, T, propagation direction polarization, elastic constants, C_{ijkl}, and density, ρ of the P42/mnm symmetry of Stishovite.

Direction of propagation	Polarization	Velocity
[100]	[100]L; [010](T); [001](T)	$V_P = \sqrt{\frac{C_{11}}{\rho}}\ V_S = \sqrt{\frac{C_{66}}{\rho}};\ V_S = \sqrt{\frac{C_{44}}{\rho}}$
[110]	[110](L); [1ī 1](T); [001](T)	$V_P = \sqrt{\frac{C_{11}+C_{12}+2C_{66}}{2\rho}};\quad V_S = \sqrt{\frac{C_{11}-C_{12}}{\rho}};\ V_S = \sqrt{\frac{C_{44}}{\rho}}$
[001]	[001](L); plane (001)(T)	$V_P = \sqrt{\frac{C_{33}}{\rho}};\ V_S = \sqrt{\frac{C_{44}}{\rho}}$

The modulus C16 is zero for crystals belonging to the P42/mnm symmetry, when the propagation is in a plane perpendicular to the quaternary axis:

$n_1 = cos\varphi, n_2 = sin\varphi, n_3 = 0 => \Gamma_{13} = \Gamma_{23} = 0$

The equations 11, 12, 14 and 16 become:

$$\Gamma_{11} = C_{11}cos^2\varphi + C_{66}sin^2\varphi \quad (17)$$

$$\Gamma_{12} = C_{16}cos2\varphi + (C_{12} + C_{66})\frac{sin2\varphi}{2} \quad (18)$$

$$\Gamma_{22} = C_{66}cos^2\varphi + C_{11}sin^2\varphi \quad (19)$$

$$\Gamma_{33} = C_{44} \quad (20)$$

In the case of a single crystal, the azimuthal anisotropies of the P and S waves are given by the following relations ([15]):

$$A_P = \frac{V_{Pmax} - V_{Pmin}}{V_P} \quad (21)$$

$$A_S = \frac{V_{Smax} - V_{Smin}}{V_S} \quad (22)$$

Where: V_{Pmax} and V_{Pmin} are the maximum and minimum of P-wave velocity relative to the propagation velocities in the other planes (e.g., [001], [110]; Table 1) or directions, respectively; Vs_{max} and Vs_{min} are the maximum and minimum S-wave velocity relative to the propagation velocities in the other planes (Table 1), respectively.

Because shear waves have two perpendicular propagation directions, two polarization anisotropy values were determined As1 and As2.

Results and Discussion

Figures 4 (V_P-pressure dependency) and 5 (Vs-pressure dependence) show the obtained body wave velocities in comparison to earlier research of [5, and 16]. Except for [16], our obtained Vs in the stishovite phase range from 0 to 30 GPa are similar to earlier investigations, exhibiting a slight rise with pressure (Fig. 4). Our obtained V_P for the V_P-P relation are considerably different from prior studies, where a kind of similarity is exhibited between them. Our V_P in the stishovite phase is lower than in prior research and increases significantly with pressure (Fig. 4). A similarity of 50 to 60 GPa is found between our results and those of [5] and [16] for V_P in the $CaCl_2$-type phase, followed by a large divergence between all the examined values, especially after 70 GPa (Fig. 4).

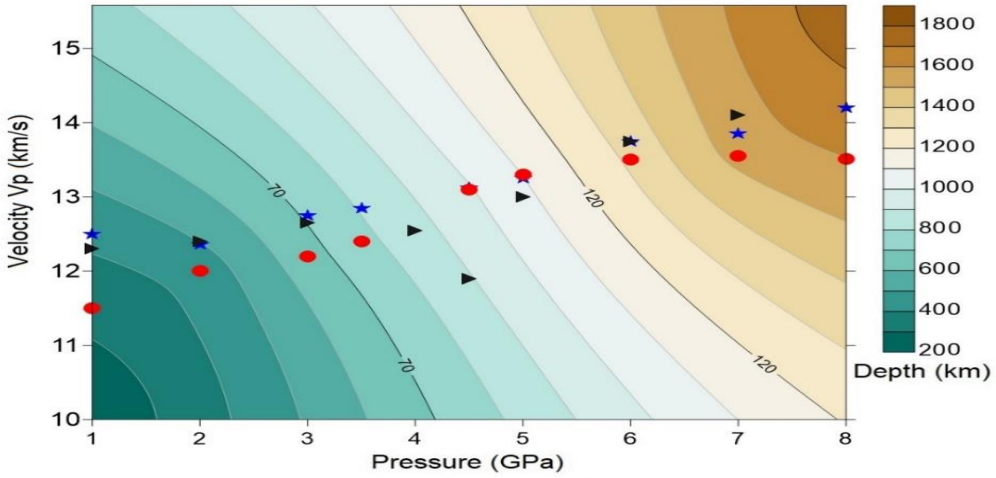

Fig. 4: P-wave velocity pressure dependence (red circles: present study; bleu stars: [5]; black triangles: [16] in stishovite and $CaCl_2$-type phases correlated to earth's depth from 200 to 1800 km using Pressure-Depth model of [20].

The pressure dependence of our computation near the phase transition (40 GPa) shows that in the stishovite phase, the increase in Vs is relatively tiny compared to V_P approximately, 7 km/s (Fig. 5). When the pressure exceeds 40 GPa, the increase becomes more visible (Fig. 5). The behavior of V_P variation with pressure is opposite; the variation is obvious from 10 to 40 GPa, where V_P varies between 11 and 12.5 km/s, and above 40 GPa, the variation changes slowly with pressure (from 13 to 13.5 km/s) (Fig. 4). This may be related to B and G pressure dependence according to formulas (1) and (2) and illustrated in Fig. 3.

Figures 6 and 7 illustrate the azimuthal anisotropies for compressional and shear waves of stishovite and $CaCl_2$-type phases, compared to [5] and [16]. In general, all values exhibited the same behavior of AP,S1,S2 in the stishovite phase: an increase with pressure followed by a quick leap around the phase transition boundary, 40-50 GPa, with increasing returns but relatively slow in the $CaCl_2$-type phase. The present study's leap is parallel to that of [16], but with a shift controlled by the phase transition, resulting in a discrepancy of 5 GPa in of the azimuthal anisotropy of the S-wave. The azimuthal anisotropy jumps of compressional wave [5] and [16] (Fig. 6) decrease slowly with pressure in the $CaCl_2$-type phase, and in our case, the AP relation increases very little, but at 70 GPa, a fast increase is observed (Fig. 6), indicating that a new material behavior occurs and can be related to the $CaCl_2$-type-seifertite transition [4].

The anisotropy computation revealed that SiO_2 is substantially anisotropic for the two phases, stishovite and $CaCl_2$-type, particularly for S-wave vs P-wave (AP) (figures 6 and 7). The azimuthal anisotropy of the S-wave fell considerably to 60% for the two propagation directions, As1 and As2 (Fig. 7), whereas the decrease for the P-wave was minimal (only 10%) (Fig. 6).

In this work, we use the pressure-depth model of [20] to correlate the V_P and Vs changes of the earth's depth and high-pressure. Figures 4 and 5 show the obtained results. These two correlations show that at 1800 km, V_P and Vs tend to decrease. Phase transition pressure of 40 GPa estimated by [13] matches to 1000 km from depth-pressure Erath's model in [7].

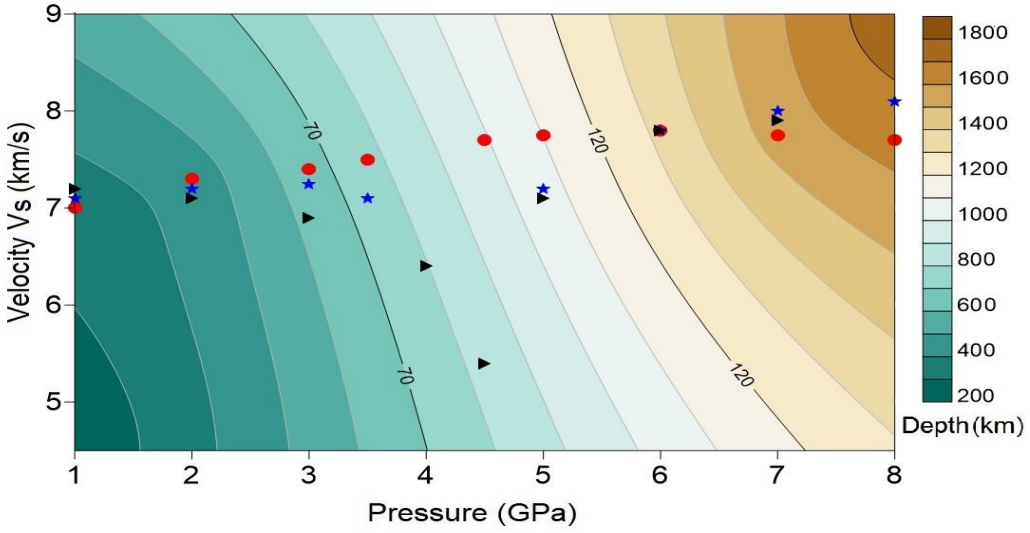

Fig. 5: S-wave velocity pressure dependence (red circles: present study; bleu stars: [5]; black triangles: [16] in stishovite and $CaCl_2$-type phases correlated to earth's depth from 200 to 1800 km using Pressure-Depth model of [20].

The pressure transition of the stishovite-$CaCl_2$-type phase, as summarized by [16], is 48 GPa and equates to 1200 km. Using the P-t figure, this depth shifts to 1400-1600 km, which includes a seismic discontinuity around Mariana Island (1670 km). Reference [3] found a shift of 68-78 GPa, which amounts to 1840 km. This depth is comprised of seismically recorded velocity scatters beneath the Tonga-Fiji and Africa areas (1400-1800 km), according to [4].

The total absence of density jump in the stishovite-$CaCl_2$-type transition boundary phase in [13] indicates that the boundary of 1000 km or more cannot be considered a seismological reflector or discontinuity as Moho, Lehmann, and D'' discontinuities in the Primitive Reference Earth Model (PREM), which agrees with the previously cited studies. The highest azimuthal anisotropy obtained for shear waves in silica (109.5% in our study and 148% discovered by [5]) must be considered in models to explain the seismic anisotropy origins suggested by [5]. This anisotropy is induced by the softening of stishovite's shear modulus under high pressure, according to [16]. Figures 6 and 7 illustrate azimuthal anisotropies connected to depth at 1000 km in S-wave velocity in the two polarization directions, As1 and As2. After this depth, anisotropy gradually rises until 1800 km for P and S-wave velocities.

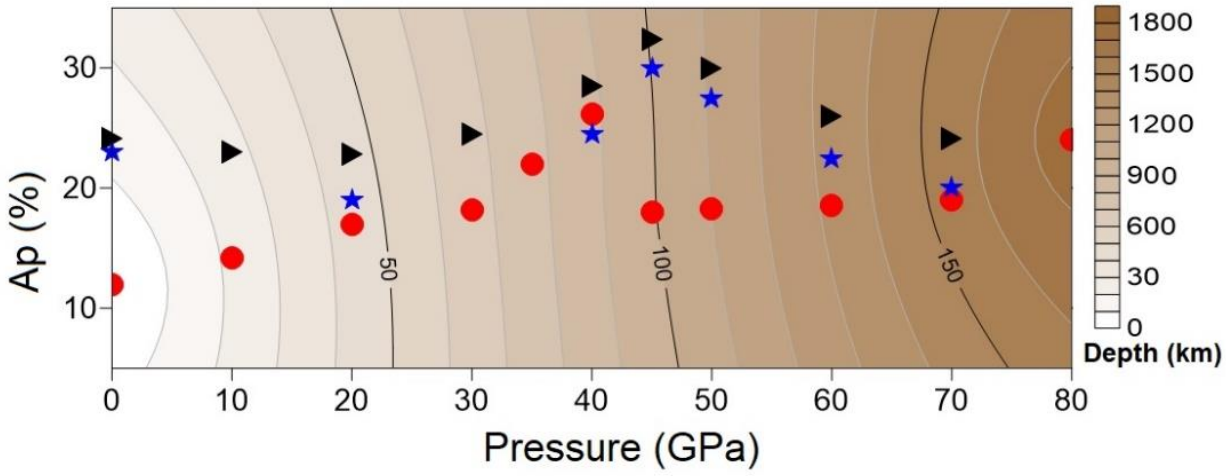

Fig. 6: Azimuthal anisotropy, A_P, in P-wave velocity pressure dependence (red circles: present study; bleu stars: [5]; black triangles: [16]) in stishovite and $CaCl_2$-type phases correlated to earth's depth from 200 to 1800 km using Pressure-Depth model of [20]. Depth contours in Fig. are divided over 10 km.

III.Conclusion

We estimated the body wave velocities of two SiO_2 polymorphs, stishovite and $CaCl_2$-type phases, at lower mantle pressures ranging from 0 to 80 GPa. We also computed the azimuthal anisotropy of P- and S-waves. According to the stishovite seismic anisotropy analysis, there is a 26% variation in V_P and a 109.5% variation in Vs. If silica exists freely in the lower mantle, this implies that there is a detectable seismic discontinuity at 40 GPa, which corresponds to a depth of 1000 km. Our geophysical calculations and prior studies taking temperature into account in the pressure phase transition of stishovite-$CaCl_2$-type revealed that the 1000-2000 km zone in the lower mantle comprises free silicate. The used method in this work allows us to investigate a pure pole in the lower mantle, SiO_2. This will allow to investigate other oxides by calculating their elastic characteristics and producing tomographic images that show the fluctuation of seismic velocities in Earth's layers example ([21, [22]).

Acknowledgements

We would like to thank the "Laboratory for Studies of Surfaces and Interfaces of Solid Materials (LESIMS)" of Ferhat Abbas University (Algeria) in particular Prof. Layachi Louail and Dr. Youcef Madhekour for providing us with the chance to compute the elastic properties using the CASTEP software license.

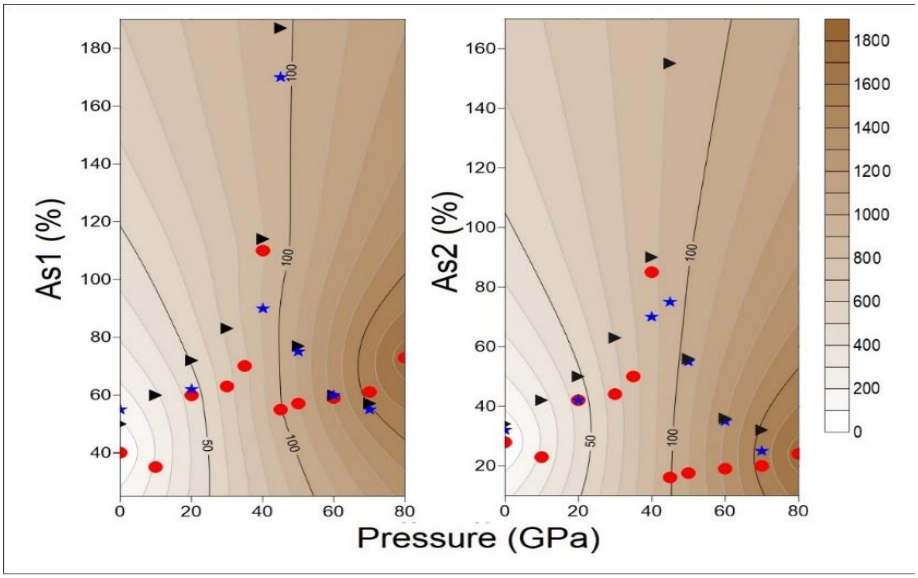

Fig. 7: Azimuthal anisotropies, As_1 and As_2, in S-wave velocity pressure dependence (red circles: present study; bleu stars: [5]; black triangles: [16]) in stishovite and $CaCl_2$-type phases correlated to earth's depth from 200 to 1800 km using Pressure-Depth model of [20]. Depth contours in figures are divided over 10 km.

References

[1] Condie K.C., Earth as an Evolving Planetary System. Second Edition, Elsevier/Academic Press, 2011.

[2] Stishov, S.M. S.V., Popova, New dense polymorphic modification of silica, Geopkhimiya, 10, 839 – 937, 1961.

[3] Fischer, R. A. A. J, Campbe. B. A., Chidester, D. M., Reaman, E. C., Thompson, P., Prakapenka, and, J.S., Smith. Equations of state and phase boundary for stishovite and $CaCl_2$-type SiO_2. American Mineralogist, Volume 103, pages 792–802, 2018.

[4] Sun, N. W., Shi, Z., Mao, C., Zhou, and V.B., Prakapenka. High Pressure-Temperature Study on the Thermal Equations of State of Seifertite and $CaCl_2$-Type SiO_2. Journal of Geophysical Research: Solid Earth 10.1029/2019JB017853.

[5] Karki, B.B. L.,Stixrude J., Crain. Ab initio elasticity of three high-pressure polymorphs, Geophysical Research Letters, 24, 3269-3272, 1997.

[6] Tsuchiya, T. R., Caracas, J., Tsuchiya. First principles determination of the phase boundaries of high-pressure polymorphs of silica, Geophysical Research Letters, 31, L11610, 2004.

[7] Karki, B.B. L., Stixrude, R.M. Wentzcovitch. High pressure elastic properties of major materials of earth's mantle from first principles, Rev Geophys., 39:507–534, 2001.

[8] Radi, Z. A.K., Yelles-Chaouche, G., Bokelmann. Seismic anisotropy of north-eastern Algeria from shear-wave splitting analysis, Phys. Earth Planet Inter. (248) 73–82,2015.

[9] Radi Z. A.K., Yelles-Chaouche, V. Corchete, S. Guettouche. Crust and upper mantle shear wave structure of Northeast Algeria from Rayleigh wave dispersion analysis, Phys. Earth Planet Inter. (270) 84-89, 2017.

[10] Radi Z., and A.K. Yelles-Chaouche, Shear velocity structure beneath Northern Algeria from Rayleigh-wave analysis, J. African Earth Sci. 186, 104446, 2022.

[11] Karki B.B., and L., Stixrude. Seismic velocities of major silicate and oxide phases of the lower mantle, Journal of Geophysical Research: Solid Earth 104 (B6), 13025-13033, 1999.

[12] Buchen, J. H., Marquardt, K., Schulze, S. Speziale, T, B., Ballaran, N., Nishiyama and M., Hanfland. Equation of State of Polycrystalline Stishovite Across the Tetragonal-Orthorhombic Phase Transition. Journal of Geophysical Research: Solid Earth 10.1029/2018JB015835.

[13] Radi, Z., S. Tlili, K. Layadi, L. Louail, A. Yells-Chaouche, Y. Madhekour, S. Guettouche. Elastic Proprieties of SiO_2 nanostructure in High-Pressure Condition, Vol.18,No. 1, January - March 2023, p. 273 - 278. DOI: 10.15251/DJNB.2023. 181.273.

[14] Blase, X. Introduction to Density Functional Theory. https://hal.archives-ouvertes.fr/hal-03070870.

[15] Wang, F. Y., Tange, T., Irifune, and K.I, Funakoshi. P-V-T-equation of state of stishovite up to mid-lower mantle conditions. Journal of Geophysical Research, 117, B06209, 2012.

[16] Yang, R. and Z., Wu, Elastic properties of stishovite and the $CaCl_2$-type silica at the mantle temperature and pressure: An ab initio investigation. Earth and Planetary Science Letters 404, 14–21, 2014.

[17] Weidner, D. J., and M. T. Vaughan, Elasticity of pyroxenes: Effects of composition versus crystal structure, J. Geophysical Research Letter, 87, p 9349, 1982.

[18] Li, B., S.M. Rigden, and R.C., Liebermann. Elasticity of stishovite at high pressure. Physics of the Earth and Planetary Interiors, 96, 113–127, 1996.

[19] Jiang, F. G.D., Gwanmesia, T.I., Dyuzheva and T.S., Duffy. Elasticity of stishovite and acoustic mode softening under high pressure by Brillouin scattering. Physics of the Earth and Planetary Interiors, 172, 235–240, 2009.

[20] Völgyesi L, Moser M (1982): The Inner Structure of the Earth. Periodica Polytechnica

[21] Chem. Eng., Vol. 26, Nr. 3-4, pp. 155-204.

[22] Radi. Z. 2016. Étude de l'anisotropie sismique du nord-Est de l'Algérie. http://dspace.univ-setif.dz:8888/jspui/handle/123456789/1584.

[23] Tlili, S., L. Louail, A. Bouguera, K. Haddadi, Y. Contribution to the study of structural and elastic properties of wüstite under pressure up to 140 GPa by pseudopotential calculations. Phase Transitions 90 (12), 1229-1240, 2017.